J. Fluid Mech. (1995), *vol.* 288, *pp.* 75–102

Fingering instabilities in vertical miscible displacement flows in porous media

By O. MANICKAM[1]† AND G. M. HOMSY[2]

[1] Department of Mechanical Engineering, Stanford University, Stanford, CA 94305, USA

[2] Department of Chemical Engineering, Stanford University, Stanford, CA 94305, USA

(Received 26 January 1994 and in revised form 17 October 1994)

The fingering instabilities in vertical miscible displacement flows in porous media driven by both viscosity and density contrasts are studied using linear stability analysis and direct numerical simulations. The conditions under which vertical flows are different from horizontal flows are derived. A linear stability analysis of a sharp interface gives an expression for the critical velocity that determines the stability of the flow. It is shown that the critical velocity does not remain constant but changes as the two fluids disperse into each other. In a diffused profile, the flow can develop a potentially stable region followed downstream by a potentially unstable region or vice versa depending on the flow velocity, viscosity and density profiles, leading to the potential for 'reverse' fingering. As the flow evolves into the nonlinear regime, the strength and location of the stable region changes, which adds to the complexity and richness of finger propagation. The flow is numerically simulated using a Hartley-transform-based spectral method to study the nonlinear evolution of the instabilities. The simulations are validated by comparing to experiments. Miscible displacements with linear density and exponential viscosity dependencies on concentration are simulated to study the effects of stable zones on finger propagation. The growth rates of the mixing zone are parametrically obtained for various injection velocities and viscosity ratios.

1. Introduction

In a displacement process the interface between the two fluids is often unstable when a fluid of higher mobility displaces a fluid of lower mobility and the resulting instabilities develop into viscous fingers. Since the early experiments and analysis of Hill (1952), there has been a tremendous growth in the literature published on viscous fingering instabilities (see Homsy 1987 for a detailed review). The problem finds application in enhanced oil recovery, groundwater flows, fixed bed regeneration, geothermal wells, etc. Besides its practical applications, the nonlinear dynamics through which the instabilities evolve are of interest from a fluid mechanics point of view as well.

In most applications, viscous fingering instabilities are undesirable as they result in a reduced sweep efficiency of the displacement process. Any process aimed toward eliminating the instabilities or controlling the growth rate of the viscous fingers is of technological importance. Manickam & Homsy (1994) analysed horizontal miscible displacements with fluid pairs that have a non-monotonic viscosity–concentration relationship and found that non-monotonocities in the spatial variation of viscosity are effective in restricting the nonlinear growth of the viscous fingers. When the viscosity

† Present address: Canon Research Center America, Inc., Palo Alto, CA, USA.

variation is non-monotonic, the flow develops an unstable zone followed downstream by a stable zone, which then acts as a barrier to the growth of the instabilities. There are other situations where a potentially stable region develops adjacent to a potentially unstable region, for example in 'Water-alternate-Gas' (WAG) schemes where the concentration of the injected fluid is varied to achieve a spatially non-monotonic viscosity profile (Christie, Muggeridge & Barley 1991). The works of Dumore (1964) and Rogerson & Meiberg (1993) have shown that we can obtain a similar situation in vertical displacement flows driven by both viscosity and density contrasts. Here we analyse vertical displacements in the presence gravity and examine the effects of the stable region on finger propagation.

Dumore (1964) observed that under suitable conditions, downward displacement flows with combined gravity and viscosity effects develop transition zones that are partly stable and partly unstable. Using arguments based on pressure gradients he derived a theoretical limit on the injection velocity at which the transition zone becomes partly unstable. Coskuner & Bentsen (1990) solved the linear stability problem by approximate methods to obtain a local stability criterion equivalent to that of Dumore (1964). Hickernell & Yortsos (1986) studied displacement processes in the absence of dispersion and showed that mobility profiles with any segment of decreasing mobility are unstable in the linear regime. They included the effects of gravity and obtained a critical injection velocity for marginally stable displacement in the small-wavenumber limit. Chikhliwala, Huang & Yortsos (1988) further confirmed that non-dispersive flows with any segment of decreasing mobility are unstable regardless of the endpoint mobility values.

Dumore (1964) carried out experiments on downward displacements to test his theoretical stability limits. His experiments confirm his theoretical finding that the stability of vertical displacements depends not merely on the endpoint values of density and viscosity but on the details of the density – and viscosity – concentration relationships. Finally we mention the vertical displacement experiments of Tiffin & Kremesec (1986), for which evaluation of stability based on endpoint properties is misleading and inaccurate. Tiffin & Kremesec attributed the curious results in their downward displacement flows to non-ideal density behaviour.

The numerical work of Rogerson & Meiberg (1993) further shows that in vertical displacements with monotonic viscosity profiles, the presence of density contrasts can introduce potentially stable zones followed downstream by potentially unstable zones or vice versa. Rogerson & Meiberg (1993) found that vertical flows with certain combinations of viscosity and density variations with concentration can develop locally stable regions, analogous to what Manickam & Homsy (1994) achieved with non-monotonic viscosity profiles in horizontal displacements. Their work demonstrates that density contrasts provide a means to control or restrict the growth of fingers in displacements with monotonic viscosity profiles.

In this paper, we analyse vertical displacement flows both in the linear and nonlinear regimes and explore the surprising similarities between vertical flows with monotonic viscosity profiles and horizontal flows with non-monotonic viscosity profiles. We first give a general treatment of the vertical miscible displacement flows with monotonic density and viscosity profiles and investigate when and how they differ from the horizontal displacements with neutrally buoyant fluids. We next perform a linear stability analysis of vertical displacements, with particular emphasis on the effects of dispersion on the stability of the flow. We use the results of the linear theory to identify regions that are potentially stable and those that are potentially unstable. We present the results of numerical simulations of vertical displacements with combinations of

viscosity and density relationships that develop locally stable and unstable zones, and study the nonlinear dynamics. Finally, we demonstrate the possibility of 'reverse fingering', where the displaced fluid fingers through the displacing fluid more easily than vice versa, through illustrative examples.

2. Problem description

A schematic of the vertical displacement flow is shown in figure 1. A fluid of viscosity μ_1 and density ρ_1 displaces another fluid of viscosity μ_2 and density ρ_2 with an injection velocity U along the direction of gravity. We work in a reference frame moving with the injection velocity U, and in the moving reference frame the governing equations in two-dimensions are

$$\frac{\partial u}{\partial x}+\frac{\partial v}{\partial y}=0, \tag{1a}$$

$$\frac{\partial p}{\partial x}=-\mu(u+U)+\rho, \tag{1b}$$

$$\frac{\partial p}{\partial y}=-\mu v, \tag{1c}$$

$$\frac{\partial}{\partial t}+u\frac{\partial c}{\partial x}+v\frac{\partial c}{\partial y}=\frac{\partial^2 c}{\partial x^2}+\frac{\partial^2 c}{\partial y^2}, \tag{1d}$$

$$\mu=\mu(c), \tag{1e}$$

$$\rho=\rho(c). \tag{1f}$$

In the above equations μ is the ratio of the viscosity to the constant permeability of the porous medium, which is simply referred to as viscosity. The viscosity is scaled with the viscosity of the displacing fluid μ_1 and the density is scaled with $\Delta\rho=\rho_2-\rho_1$. The velocity, length and time are scaled with V_{ch}, D/V_{ch} and D/V_{ch}^2 respectively, where the characteristic velocity $V_{ch}\equiv|\Delta\rho|\,g/\mu_1$. We choose to scale the velocities with V_{ch} rather than the injection velocity U because in the presence of density contrasts we can have a non-trivial flow even when $U=0$. The concentration of the fluid at $x=-\infty$ is taken to be 1 and that at $x=+\infty$ is taken to be 0. All the velocities in (1) are volume-averaged and (1*a*) represents conservation of volume. If mass-averaged velocities instead of volume-averaged velocities are used, then the velocity field will not in general be divergent-free as noted by Joseph (1990). However, an appeal to Boussinesq approximation establishes an equivalence between volume- and mass-averaged formulations. In addition, a variety of comparisons between predictions based on (1) and laboratory experiments (Christie *et al.* 1989; Tchelepi *et al.* 1993, and the validation studies of § 5.1) confirm that the governing equations (1) adequately describe the physics of the displacement process.

We assume that the density varies linearly with concentration. Most fluid pairs have a linear density–concentration relationship and any deviations from a linear relationship is due to volume change of mixing. The conservation of volume equation (1*a*) assumes that there is no volume change of mixing and thus a linear density profile is consistent with this assumption. We use the following normalized linear density profile:

$$\rho(c)=\begin{cases} c & \text{if} \quad \rho_1>\rho_2 \\ 1-c & \text{if} \quad \rho_1<\rho_2. \end{cases} \tag{2}$$

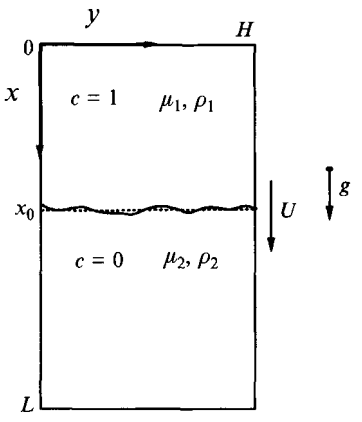

FIGURE 1. Schematic of vertical miscible displacement.

When $\rho_1 > \rho_2$, the flow is gravitationally unstable and when $\rho_1 < \rho_2$, the flow is gravitationally stable. We use the following exponential viscosity profile for most of our study:

$$\mu(c) = e^{R(1-c)}. \tag{3}$$

This profile is the same as that used by Tan & Homsy (1986) and other investigators (Yortsos & Zeybek 1988; Zimmerman & Homsy 1992; Rogerson & Meiburg 1993). It closely represents the 'quarter-power mixing rule' popularly employed by petroleum engineers (Tiffin & Kremesec 1986; Fayers & Newley 1988) to describe the viscosity–concentration relationship.

When $R > 0$ the flow is viscously unstable and when $R < 0$ the flow is viscously stable. We further restrict our attention to downward displacements, i.e. flows with $U > 0$ in the coordinate system shown in figure 1. We can confine our attention to downward displacements without loss of generality because for every upward displacement we can find an 'equivalent' downward displacement, so long as the density profile is linear. We establish this in the next section where we discuss at length the 'equivalence' between flows.

3. Equivalent flows

Two flow problems are said to be *equivalent* if the solution to one can be obtained from the other through simple transformations. The equivalence between flows not only reduces the number of flow configurations to be independently analysed but also helps understand the underlying differences between flow problems. We first examine the conditions under which a vertical displacement with density contrast is different from a horizontal displacement with neutrally buoyant fluids.

In immiscible displacements it can be shown that all vertical flows have an equivalent horizontal flow (Tryggvason & Aref 1983). When the two fluids are miscible however, this is not always true. Tan (1987) in his analysis of miscible displacements showed that when the variation of fluid properties with concentration is small, the density-driven instability is analogous to the viscous-driven instability. What is the general criterion for a vertical displacement to be equivalent to a horizontal displacement? An examination of the right-hand side of (1*b*) reveals that when the viscosity and the density profiles are linearly related, i.e. if $\mu(c) = C_1\rho(c) + C_2$ for some constants C_1 and C_2, then a vertical displacement with density contrast has an equivalent horizontal displacement and vice versa.

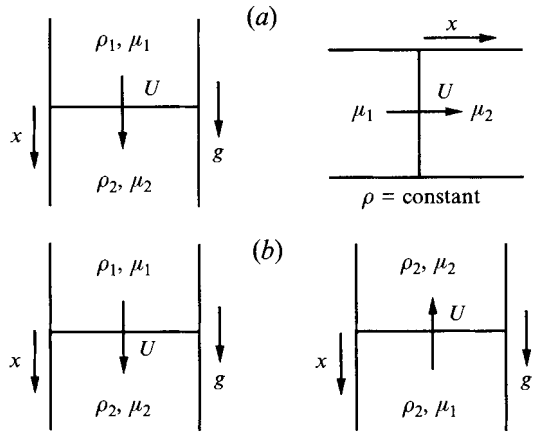

FIGURE 2. (*a*) The vertical displacement has an equivalent horizontal displacement when the density and viscosity profiles are linearly related. (*b*) The downward displacement and the upward displacement are equivalent when the density profile is linear.

When the viscosity and density profiles are both linear, a vertical displacement has an equivalent horizontal displacement. Consider the two displacements shown in figure 2(*a*) – the vertical displacement where both the viscosity and density profiles are linear and the horizontal displacement with the same linear viscosity profile but with neutrally buoyant fluids. It is straightforward to show that the two flows are equivalent and the solution to the vertical displacement v (scaled with $V_{ch} \equiv \Delta\rho g/\mu_1$) can be obtained from those of the horizontal displacement h (scaled with U_h) through the transformations

$$U_v = \gamma + U_c, \tag{4a}$$

$$u_v(x, y, t) = \gamma u_h(\gamma x, \gamma y, \gamma^2 t), \tag{4b}$$

$$v_v(x, y, t) = \gamma v_h(\gamma x, \gamma y, \gamma^2 t), \tag{4c}$$

$$c_v(x, y, t) = c_h(\gamma x, \gamma y, \gamma^2 t), \tag{4d}$$

$$p_v(x, y, t) = p_h(\gamma x, \gamma y, \gamma^2 t) + (-\mu_2 U_c + \rho_2)\, x, \tag{4e}$$

where $\gamma = \mu_1 U_h/\Delta\rho g$ and $U_c = (\rho_2 - \rho_1)/(\mu_2 - \mu_1)$, $\mu_2 \neq \mu_1$. The solutions to the vertical displacements are scaled with the characteristic velocity $V_{ch} \equiv \Delta\rho g/\mu_1$ while the solutions to the horizontal displacements are scaled with the injection velocity U_h, and the scaling factor γ is the ratio of the two velocities $\gamma = U_h/V_{ch}$. A vertical displacement with linear viscosity and density profiles and an injection velocity U_v' (prime indicates unscaled quantities) is equivalent to the horizontal displacement with the same linear viscosity profile and an injection velocity $U_h = U_v' - U_c'$ where U_c', as we will later see in §4.1, is the critical velocity when both the density and viscosity profiles are linear.

In dilute solutions, the variations of fluid properties are small, so that they can be treated as linear and hence vertical displacements with such solutions are equivalent to the horizontal displacements with neutrally buoyant fluids. For most fluid pairs, the density profile is linear while the viscosity profile is nonlinear and consequently the vertical displacements are expected to be different from such horizontal displacements. The density contrast will have an effect on the flow when the injection velocity is such that $\mu_{min}\, U/\Delta\rho g \lesssim O(1)$ where $\mu_{min} = \min(\mu_1, \mu_2)$. According to our scaling, this condition amounts to $U \lesssim O(1)$ when $\alpha = \mu_2/\mu_1 > 1$ and $U \lesssim O(1/\alpha)$ when $\alpha < 1$, where U is the injection velocity scaled with V_{ch}.

When the density profile is linear, every upward displacement has an equivalent downward displacement and vice versa. Consider the two displacements shown in

figure 2(*b*) – with the downward and upward displacements denoted by *d*, *u*. If the velocities are uniformly scaled with $V_{ch} = \Delta\rho g/\mu_1$ for the two problems, so that $U_u = -U_d$, $\mu_u(c) = \mu_d(1-c)$ and $\rho_u(c) = \rho_d(c)$, then the solutions to the upward displacement can be obtained from those of the downward displacement through the following simple transformations:

$$u_u(z, y, t) = -u_d(-x, y, t), \tag{5a}$$

$$v_u(x, y, t) = v_d(-x, y, t), \tag{5b}$$

$$c_u(x, y, t) = 1 - c_d(-x, y, t), \tag{5c}$$

$$p_u(x, y, t) = p_d(-x, y, t) + x. \tag{5d}$$

The above transformations can easily be verified by substituting them into (1). When the two fluids are immiscible, the downward displacements always have an equivalent upward displacement (Tryggvason & Aref 1983) whereas when the two fluids are miscible, the equivalence holds only when the density profile is linear (or if the density profile is such that $\rho(1-c)+\rho(c) = 1$.) For fluid pairs with a nonlinear density–concentration relationship, upward displacements are not equivalent to downward displacements and the two cases need to be studied independently. Non-ideal density behaviour in the experiments of Tiffin & Kremesec (1986) resulted in upward displacements being significantly different from downward displacements. As we assume a linear density profile (2), it is sufficient to consider only the downward flows and the solutions to the upward displacements can be obtained using (5).

4. Linear stability analysis

We begin our study by analysing the stability of vertical miscible displacements. We assume the porous medium to be of infinite extent in all directions and that at $t = 0$, the two fluids are separated by a sharp interface located at $x = 0$. The base state solutions to such flows in a coordinate system moving with the injection velocity are

$$\bar{u} = 0; \quad \bar{c} = \tfrac{1}{2}\mathrm{erfc}\left(\frac{x}{2t^{1/2}}\right). \tag{6}$$

The base flow is time dependent and we follow the approach of Tan & Homsy (1986) by making a quasi-steady-state approximation. We assume that the perturbations grow or decay faster than the rate at which the base state changes, which allows us to freeze the base state solution (6) at time t_0 and treat the flow as though it were steady. The initial value calculations of Tan & Homsy have validated this approach except for a short time when the base state changes rapidly. The governing equations (1) are perturbed and linearized and solutions of the following form are sought for the perturbations in concentration and velocity:

$$(c', u') = (\phi_c, \phi_u)\exp(iky + \sigma(t_0)\,t), \tag{7}$$

where σ is the growth rate and k is the wavenumber of the perturbations. The flow is stable when $\mathrm{Re}(\sigma) < 0$ for all k and is unstable otherwise. The resulting eigenvalue problem is (Coskuner & Bentsen 1990; Bacri, Salin & Yortsos 1992)

$$\left(\frac{\mathrm{d}^2}{\mathrm{d}x^2} - \sigma - k^2\right)\phi_c = \frac{\mathrm{d}\bar{c}}{\mathrm{d}x}\phi_u, \tag{8a}$$

$$\left(\frac{\mathrm{d}}{\mathrm{d}x}\left(\bar{\mu}\frac{\mathrm{d}}{\mathrm{d}x}\right) - \bar{\mu}k^2\right)\phi_u = k^2\left[U\frac{\mathrm{d}\mu}{\mathrm{d}c} - \frac{\mathrm{d}\rho}{\mathrm{d}c}\right]\phi_c. \tag{8b}$$

When the third dimension is included, the linear stability equations are still the same as (8) with $k^2 = k_y^2 + k_z^2$, where k_y and k_z are the wavenumbers of the perturbations in the y- and z-directions respectively. The eigenvalue problem (8) is a fourth-order system with coefficients that vary with both space and frozen time t_0. Coskuner & Bensten (1990) solved the linear problem by assuming the coefficients of equation (8) to be constants. They argue that such approximations yield a local result, which they use to obtain a global stability condition. Bacri *et al.* (1992) derived an analytical solution at $t_0 = 0$ when the two fluids are separated by a sharp interface, which is discussed in §4.1.

The solutions to the eigensystem (8) have both a discrete and continuous eigenvalue spectrum. The discrete modes satisfy the decay conditions while the continuous modes remain bounded as $x \to \pm\infty$. The complete eigenvalue spectrum is discussed in Manickam & Homsy (1993) and Manickam (1994). The eigensystem (8) can be solved analytically for a step concentration profile, i.e. when $t_0 = 0$. Asymptotic expansions are possible in the small-wavenumber limit ($k \ll 1$). For a finite t_0 and k, we resort to finite difference techniques to solve (8). We present the complete solutions to the eigensystem (8) in an infinite domain in the rest of this section. We first obtain the global stability criterion as a function of the frozen time t_0 and later discuss the local stability of the flow.

4.1. *Analytical and asymptotic solutions*

The analytical and asymptotic solutions obtained by Manickam & Homsy (1993) for horizontal flows are easily extended to vertical flows by repeating their derivation with the gravity term in place. Their step profile result at $t_0 = 0$ extended to the vertical flow gives the following expression for $\sigma(t_0 = 0)$ (Bacri *et al.* 1992):

$$\text{for } \Lambda_v > 0: \quad \sigma(t_0 = 0) = \tfrac{1}{2}(\Lambda_v k - k^2 - k(k^2 + 2\Lambda_v k)^{1/2}), \tag{9}$$

where $\Lambda_v = \Lambda(U - U_c)$ and

$$\Lambda = -\left(\frac{(\mathrm{d}\mu/\mathrm{d}c)_{c=0} + (\mathrm{d}\mu/\mathrm{d}c)_{c=1}}{\alpha + 1}\right); \quad \alpha = \frac{\mu_2}{\mu_1},$$

$$U_c = \frac{(\mathrm{d}\rho/\mathrm{d}c)_{c=0} + (\mathrm{d}\rho/\mathrm{d}c)_{c=1}}{(\mathrm{d}\mu/\mathrm{d}c)_{c=0} + (\mathrm{d}\mu/\mathrm{d}c)_{c=1}}.$$

The parameter Λ has the same definition as in Manickam and Homsy (1993) and U_c is the 'modified' critical velocity. The sign of $\Lambda_v = \Lambda(U - U_c)$ determines the stability of the flow, with stability when $\Lambda(U - U_c) < 0$ and instability when $\Lambda(U - U_c) > 0$. When the dependences of viscosity and density on concentration are linear, the critical velocity U_c given by (9) reduces to that obtained by Hill (1952), namely $U_c = (\rho_2 - \rho_1)/(\mu_2 - \mu_1)$.

For flows with monotonic viscosity and density profiles, the step profile result implies that when both viscosity and density contrasts have a destabilizing effect ($\mu_1 < \mu_2, \rho_1 > \rho_2$), the flow is unstable for all $U > 0$ and when they both have a stabilizing effect ($\mu_1 > \mu_2, \rho_1 < \rho_2$), the flow is stable for all $U > 0$. The interesting combinations are those where the viscosity and density differences have opposite effects. From the stability criterion $\Lambda(U - U_c) < 0$ we see that when $\mu_1 > \mu_2$ and $\rho_1 > \rho_2$ ($\mu_1 < \mu_2$ and $\rho_1 < \rho_2$), the flow is unstable (stable) when the injection velocity U is below the critical velocity U_c and is stable (unstable) when the injection velocity exceeds the critical velocity.

The step profile result (9) accounts only for the endpoint properties. Further the quasi-steady-state approximation we have made is questionable at $t_0 = 0$ when the base state changes rapidly. To understand the stability of the flow at a larger time t_0, we use the small-wavenumber expansion which is valid for all t_0. Hickernell & Yortsos (1986) obtained the small-k expansion of σ in the absence of physical dispersion. Manickam & Homsy (1993) showed that physical dispersion in the transverse direction is not important in the small-wavenumber limit but dispersion in the longitudinal direction needs to be included in the analysis. Manickam & Homsy derived the first two non-trivial terms in the small-wavenumber expansion of σ for horizontal flows. The small-k expansion involves expanding the eigensolutions in five different regions and matching them in the four overlap zones. Their results are easily extended to vertical flows by replacing $\mathrm{d}\mu/\mathrm{d}c$ and A in their solution with $U\,\mathrm{d}\mu/\mathrm{d}c - \mathrm{d}\rho/\mathrm{d}c$ and $A_v = A(U-U_c)$ respectively. We refer the reader to Manickam (1994) for details of the derivation and present here only the final result that is relevant to our discussion. The small-k expansion of the growth rate σ for $A_v > 0$ is

$$\sigma = \tfrac{1}{2}A_v k - \left(1 + \frac{\mathscr{I}(t_0)}{2(1+\alpha)}\right)(\tfrac{1}{2}A_v)^{1/2}k^{3/2} + O(k^2), \tag{10}$$

where

$$\mathscr{I}(t_0) = \int_{-\infty}^{+\infty}\left(U\frac{\mathrm{d}\mu}{\mathrm{d}c} - \frac{\mathrm{d}\rho}{\mathrm{d}c} + \tfrac{1}{2}(\alpha+1)A_v\right)\mathrm{d}x$$

and

$$c = \tfrac{1}{2}\mathrm{erfc}\left(\frac{x}{2t_0^{1/2}}\right); \quad \alpha = \frac{\mu_2}{\mu_1}.$$

The first term is independent of t_0 and thus when $A_v = A(U-U_c) > 0$ the flow that is unstable at $t_0 = 0$ will continue to remain unstable at all times. Thus $A_v > 0$ is a sufficient condition for the flow to be unstable. When $A_v < 0$, there are no positive eigenvalues and the flow is stable in the small-wavenumber limit. But to establish that the flow is stable we need to examine all wavenumbers. The question still remains: will the flow that is stable at $t_0 = 0$ remain stable at all times? In horizontal flows, Manickam & Homsy (1993) found that when $\mu(c)$ is non-monotonic, the flows that are stable at $t_0 = 0$ will eventually become unstable as the two fluids disperse into each other. It remains to be seen whether diffusion has a similar destabilizing effect on vertical flows with monotonic viscosity profiles. We solve the eigenvalue system (8) for a finite time t_0 and a finite wavenumber k, using the standard finite difference method (Manickam 1994), to understand the effects of diffusion on the stability of the flow.

4.2. *Effects of diffusion*

We consider a vertical displacement which is gravitationally unstable but viscously stable and illustrate the effects of diffusion on such flows through a specific example. We assume a linear density profile (2) with $\rho_1 > \rho_2$ and an exponential viscosity profile (3) with $R = -3$. For this combination of density and viscosity profiles, the modified critical velocity U_c given by (9) is 0.635. The flow is stable when $U > U_c$ and is unstable when $U < U_c$. We choose the three values 0.25, 0.635 and 2 for the injection velocity U so that $U < U_c$, $U = U_c$ and $U > U_c$ for the three cases respectively. We solve the system of equations (8) numerically using finite difference techniques to obtain the dispersion relation $\sigma(k; t_0)$ for each of the three cases. The results are presented in figure 3(*a–c*).

When $U < U_c$ (figure 3*a*), the numerical solution agrees with the step solution (9) at $t_0 = 0$. At $t_0 > 0$, the two fluids disperse into each other and the instabilities are

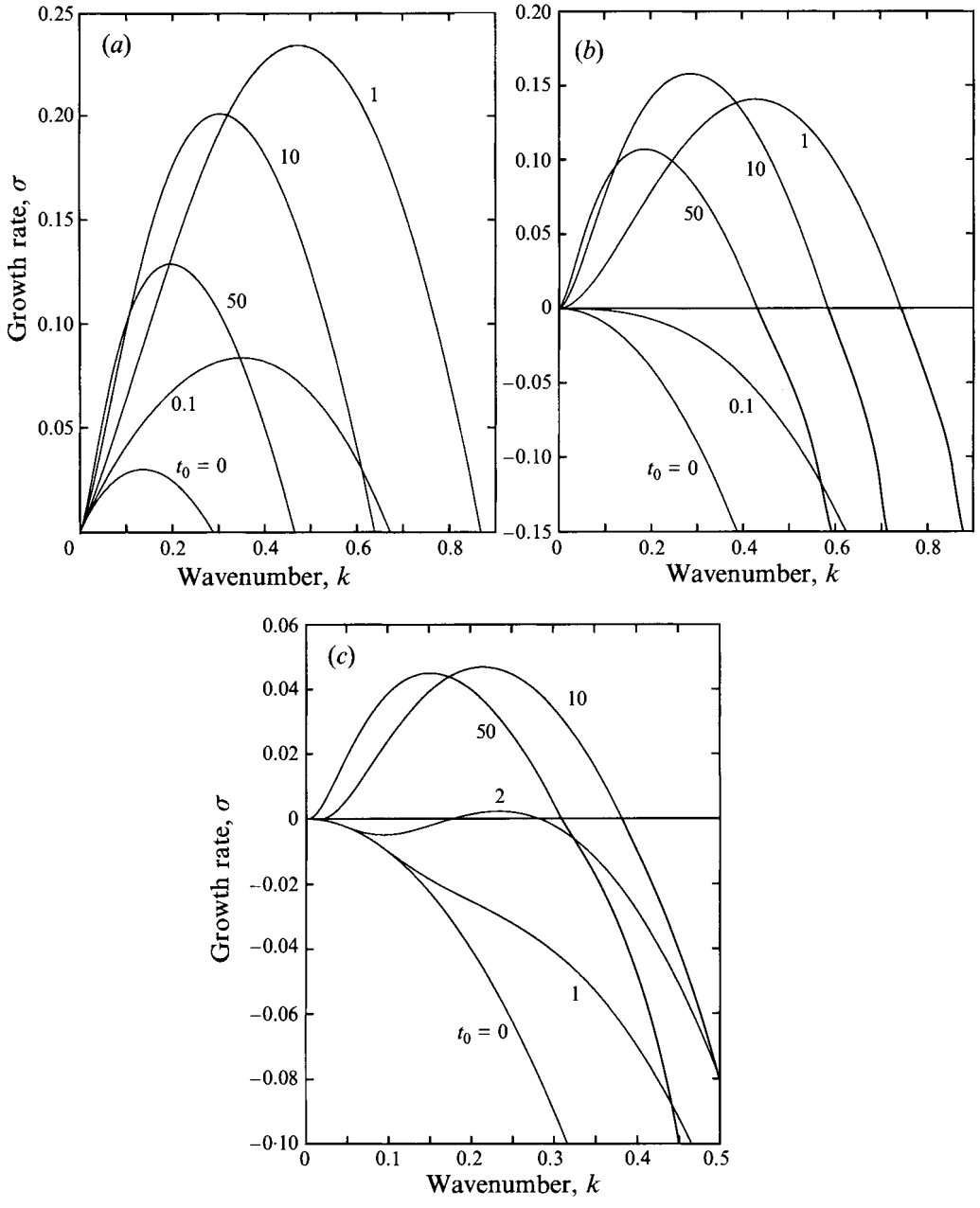

FIGURE 3. The dispersion relation $\sigma(k)$ at various frozen time t_0 for flows with $\rho_1 > \rho_2$, $\mu_1 > \mu_2$ and the three injection velocities (*a*) $U = 0.25$, (*b*) $U = 0.635$, (*c*) $U = 2$.

enhanced at short times and are mitigated at larger times. The flow is unstable at all times as predicted by the small-wavenumber expansion (10). When $U > U_c$ (figure 3*c*) the flow is stable at $t_0 = 0$ in agreement with the step profile result (9). But the flow remains stable only for a short time and as we see in figure 3(*c*) the flow has become unstable when $t_0 = 2$. In figure 3(*b*), where $U = U_c$ we see a similar destabilizing effect of diffusion.

The effects of diffusion seen in figure 3(*a–c*) are reminiscent of the effects of diffusion

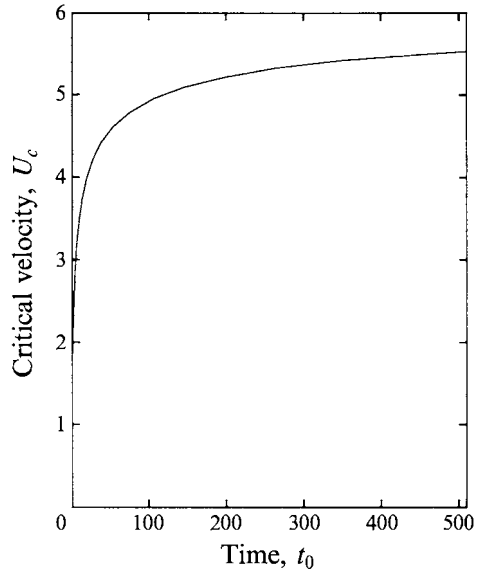

FIGURE 4. Critical velocity as a function of the frozen time t_0 for the flow with a linear density profile ($\rho_1 > \rho_2$) and an exponential viscosity profile ($\mu_1 > \mu_2$).

in horizontal flows with non-monotonic viscosity profiles (Manickam & Homsy 1993). The unstable step profiles remain unstable at all times whereas the stable ones can become unstable as diffusion progresses. In general, diffusion is expected to mitigate the instabilities and the step profile analysis is considered as the worst case. This is an example where the step profile results are misleading and should be interpreted with caution.

The fact that flows with $U \leqslant U_c$ (figure 3*b*, *c*) that are stable at $t_0 = 0$ become unstable at a later time t_0 implies that the critical velocity U_c is not a constant but varies with the frozen time t_0. We define the critical velocity at any given time t_0 as that velocity beyond which $\sigma(k) \leqslant 0$ for all modes $k \geqslant 0$. For the linear density profile (2) with $\rho_1 > \rho_2$ and an exponential viscosity profile (3) with $R = -3$, the critical velocity as a function of the frozen time, $U_c(t_0)$, is numerically calculated and the result is shown in figure 4. For this combination of $\rho(c)$ and $\mu(c)$, $A < 0$ and from the asymptotic expansion (10), we see that flows with $U < U_c(t_0 = 0)$ will remain unstable at all t_0 and hence $U_c(t_0 = 0)$ is a lower bound on the critical velocity $U_c(t_0)$. It is not surprising then that the critical velocity increases with time t_0 in figure 4. For flows that are gravitationally stable ($\rho_1 < \rho_2$) and viscously unstable ($\mu_1 < \mu_2$), $U_c(t_0 = 0)$ is an upper bound and the critical velocity decreases with t_0.

For horizontal displacements, Manickam & Homsy (1993) reported that when $\mu(c)$ is non-monotonic, the displacements that are stable at short times will become unstable if diffusion acts on the flow for a sufficiently long time. When do stable vertical flows with monotonic viscosity and density profiles become unstable? We examine this issue next through the concept of local stability.

4.3. *Local stability*

When the two fluids disperse into each other, we can conceptually think of the diffused profile as being made of infinite number of infinitesimally small steps and apply the step profile result (9) to each of these infinitesimal steps. We define a *local* critical velocity

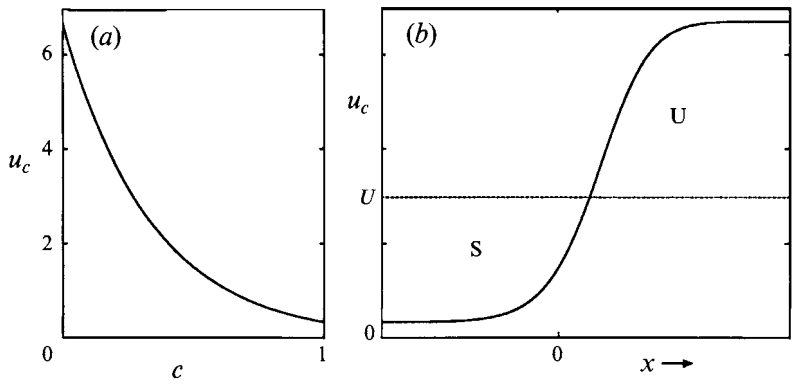

FIGURE 5. (*a*) The variation of local critical velocity u_c with concentration c and (*b*) the spatial variation of the local critical velocity $u_c(x)$ under one-dimensional dispersion. A stable region, labelled S, is followed downstream by an unstable region, labelled U, if the injection velocity U is between the lower and upper limits of the local critical velocity.

u_c as the limiting value of the step profile critical velocity given in (9) when applied to each of the infinitesimally small steps:

$$u_c(c) = \frac{\mathrm{d}\rho/\mathrm{d}c}{\mathrm{d}\mu/\mathrm{d}c}. \tag{11}$$

The local critical velocity u_c depends only on the local composition of the fluid c. A direct comparison of the injection velocity and the local critical velocity will determine the regions that are potentially unstable and those that are potentially stable. The unstable regions are regions where $U < u_c$ if $\partial\mu/\partial x > 0$ and $U > u_c$ if $\partial\mu/\partial x < 0$. The variation of the local critical velocity u_c with concentration c is plotted in figure 5(*a*) for the flow with an unstable density contrast, $\Delta\rho > 0$, and an exponential viscosity profile with a favourable viscosity ratio $\alpha = \mu_2/\mu_1 = 0.1$. The corresponding spatial variation if the flow were to disperse in a one-dimensional fashion is shown in figure 5(*b*). By comparing the *local* critical velocity with the injection velocity U we can demarcate regions that are locally stable from those that are locally unstable as indicated in figure 5(*b*). The situation is analogous to horizontal flows with non-monotonic viscosity profiles (Manickam & Homsy 1994) where the flow develops potentially unstable and stable regions adjacent to each other.

When the flow is locally stable everywhere, it will remain stable at all times. On the other hand, if the flow is locally unstable in some region, then the flow will either always be unstable or will eventually become unstable if diffusion acts on the flow for a sufficiently long time. The stability criterion for downward displacements is as follows. When $\rho_1 > \rho_2$ and $\mu_1 > \mu_2$, the flow has the potential to become unstable when $U < u_{cu}$ and when $\rho_1 < \rho_2$ and $\mu_1 < \mu_2$, the flow has the potential to become unstable when $U > u_{cl}$, where u_{cu} and u_{cl}, are, respectively, the upper and lower bounds of the local critical velocity $u_c(c)$ defined in (11). The latter condition is identical to the stability criterion obtained by Dumore (1964) who referred to the lower limit of the local critical value as $u_{st} \equiv (\mathrm{d}\rho/\mathrm{d}\mu)_{min}$.

Dumore (1964) conducted experiments where a solvent is injected vertically downward in a porous medium saturated with a denser and more viscous oil. He observed the flow to become unstable when the injection exceeded the lower limit of the critical velocity, u_{cl}. In general, u_{cl} is far below the critical velocity obtained using a step profile analysis, $U_c(t_0 = 0)$ given in (9). It is interesting to note that Hill (1952),

in his experiments with downward displacement flows, obtained favourable comparisons between his experimentally obtained critical velocities and the corresponding step profile result. Hill used dilute solutions in his experiments for which the property variations are almost linear. When both density and viscosity profiles are linear, the critical velocity is independent of concentration, $u_c(c)$ = constant, and the upper and lower bounds on the critical velocity coincide with the step profile result, namely $(\rho_2-\rho_1)/(\mu_2-\mu_1)$. This explains the good agreement between his experiments and the step profile result.

When the flow evolves into the nonlinear regime, we can still identify regions that are potentially stable and regions that are potentially unstable by comparing the *local* total velocity, rather than the injection velocity, with the *local* critical velocity. This simple method to identify regions that are locally stable and locally unstable, though not strictly valid in the nonlinear regime, serves as a useful tool to interpret the dynamics of finger propagation. We use this method extensively in the next section where we examine through direct numerical simulations, the nonlinear evolution of fingering instabilities and the influence of locally stable zones on finger propagation.

5. Numerical simulations

We use a Hartley-transform-based (Bracewell 1984, 1986; Buneman 1987) pseudo-spectral method to numerically simulate the miscible displacement flow. The method is similar to that used by Zimmerman & Homsy (1991) and Manickam & Homsy (1994). A detailed description of the method is in Manickam (1994). Zimmerman & Homsy (1992) and Tchelepi *et al.* (1993) have shown that simulations in two dimensions capture all the essential physical mechanisms through which fingers propagate in a homogeneous three-dimensional porous medium with neutrally buoyant fluids. The averaged quantities exhibit the same behaviour in two-dimensional and three-dimensional simulations. These findings are applicable to vertical displacements so long as the injection velocity is aligned with the direction of gravity. We carry out our simulations in two dimensions with the expectation that the results for averaged quantities will not be different when the third dimension is included as well. It should be noted, however, that when the fluid is injected at an angle to the direction of gravity, the two-dimensional results will be different from the three-dimensional results (Tchelepi & Orr 1993).

A schematic of the computational domain used in our simulations is shown in figure 1. The velocity, length and time are scaled with V_{ch}, D/V_{ch} and D/V_{ch}^2 respectively, where $V_{ch} \equiv \Delta\rho g/\mu_1$, unless otherwise stated. As before we work in a coordinate system moving with the injection velocity U. The non-dimensionalized width of the computational domain takes the form of a Péclet number $Pe = HV_{ch}/D$ and the aspect ratio of the domain is $A = L/H$. All our computations are carried out on the CRAY Y-MP. The typical mesh sizes we use are 128×128 and 256×256. The execution time varies depending on the problem and ranges between a few CPU minutes and about 1 CPU hour on the CRAY Y-MP.

5.1. *Gravitational fingers*

We first simulate the evolution of fingers driven solely by density differences and compare the results with the experiments of Wooding (1969). We use the simulation results to validate our code and also to understand the underlying differences, if any, between gravitational fingers and viscous fingers. Wooding (1969) observed the growth of fingers at the diffusing interface between two fluids that have the same viscosity

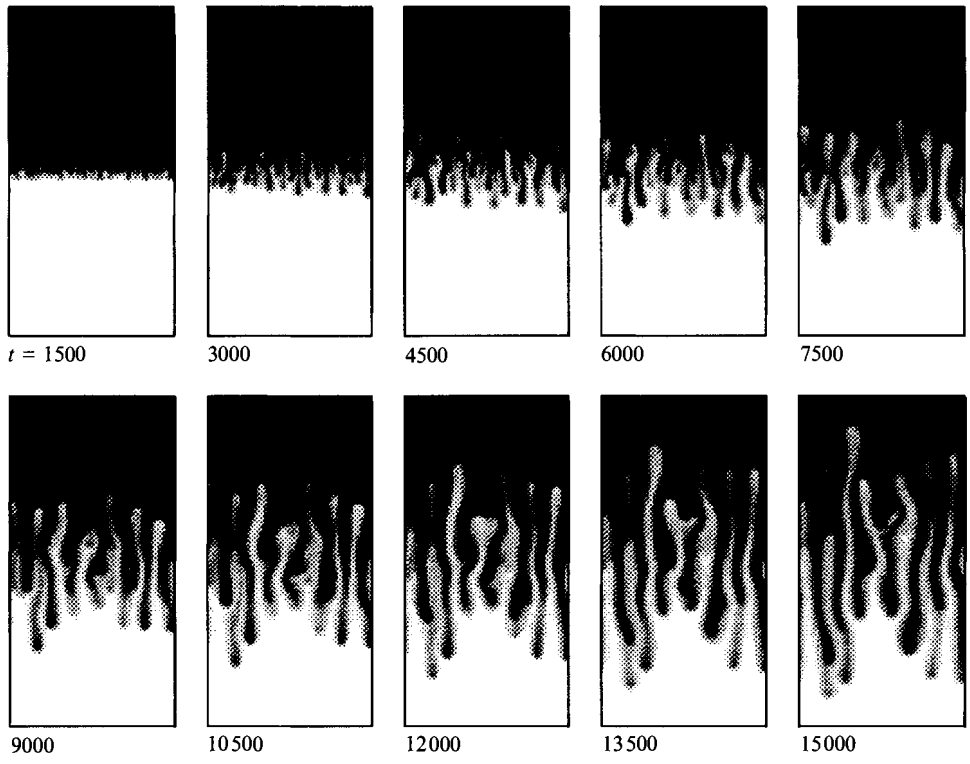

FIGURE 6. Simulation of fingers driven solely by density contrasts. The concentration field at various times are shown as grey-scale plots with the heavier fluid coloured black and the lighter fluid coloured white. The width of the computational domain is $Pe = V_{ch} H/D = 5000$ and the aspect ratio is $A = 2$.

($\mu(c)$ = constant) and a linear density profile ($\rho_1 > \rho_2$) in a Hele-Shaw cell. If we assume a constant isotropic dispersion then the only parameter of the problem is the width of the experimental cell *Pe*. If *Pe* is large enough so that the boundary effects are small, then the problem is parameterless and the averaged quantities like the mixing lengths are largely independent of *Pe* (Tan & Homsy 1988). In the Hele-Shaw cells of Wooding's experiment, the dispersion is anisotropic due to Taylor dispersion, especially when the characteristic velocity of the flow is high. However there is ample evidence in the work of Zimmerman & Homsy (1991) to suggest that some of the averaged quantities like the asymptotic growth rates of the mixing zones are not only independent of *Pe* but also of any anisotropy in the flow. Thus to compare our simulation results with Wooding's experiments, it is sufficient to simulate with a much lower *Pe* than the actual experiments and assume a constant isotropic dispersion.

We simulate a flow with constant viscosity, driven solely by an unstable density stratification in a computational domain of width $Pe = 5000$. The results of the simulations are presented in figure 6. The simulations are with a much smaller cell width and for a much shorter time than the experiments of Wooding. However, the finger patterns in figure 6 are strikingly similar to those seen in the experiments of Wooding (figure 2*b* in Wooding 1969). We observe the nonlinear fingering mechanisms of spreading, shielding, coalescence, and tipsplitting described by Tan & Homsy (1988), at both ends of the fingered zone. The feature that is noteworthy is that the density-driven fingers, unlike their viscosity-driven counterparts, have *no preferred direction of propagation*. When the density profile is linear, the lighter fluid rises into

the heavier fluid as rapidly and through the same fingering mechanisms as the heavier fluid sinks into the lighter fluid. The up–down symmetry of the fingering instabilities in the absence of viscosity contrast was noted by Tryggvason & Aref (1983) for immiscible displacements. That the gravitational fingers propagate at the same rate in either direction is not very surprising in light of our discussions of equivalent flows in §3. If we start our simulations shown in figure 6 with $u(-x, y, t = 0)$ instead of $u(x, y, t = 0)$, then we would obtain the exact mirror image of the concentration fields shown in figure 6, i.e. $1-c(-x, y, t)$. This can easily be verified from the governing equations (1) when $U = 0$, $\mu(c) =$ constant and the density profile is linear (more generally when $U = 0$, $\mu(1-c) = \mu(c)$ and $\rho(1-c)+\rho(c) = 1$).

Wooding (1969) has measured the mean wavelength and the mean amplitude of the fingers at various times t in his experiments. His measurements of mean wavelengths asymptote to $\sim t^{1/2}$ while those of mean amplitudes asymptote to $\sim t$. The only meaningful quantitative comparisons we can make are with these asymptotic variations in time. Wooding obtained the mean amplitude by measuring the crest to trough distance from photographs of the Hele-Shaw cell at various times and the mean wavelength by visually counting the number of fingers (the average of the number of crests and troughs) and dividing the width of the cell by it. We compare our simulation results against these two measurements.

Wooding reported that one half of the mean crest to trough amplitude Z_m, when scaled with the diffusion coefficient and a characteristic velocity, asymptotes to $0.442t$. Noting that the characteristic velocity used by Wooding is one-half of the characteristic velocity we use, the mean crest to trough amplitude ($2Z_m$) from Wooding's experiment when scaled with $V_{ch} \equiv \Delta\rho g/\mu_1$ asymptotes to a rate of 0.442. The mean crest to trough amplitude is a measure of the length of the fingered zone and its growth is similar to that of the mixing length, defined as the distance in which the transversely averaged concentration varies from 95% to 5%. The mixing lengths obtained from our simulations asymptote to a growth rate of ≈ 0.5, which compares favourably with the experimental value of 0.442. The mean wavelength, λ, in Wooding's experiment when scaled with the characteristic velocity and transverse diffusivity asymptotes to $\lambda/2\pi \sim 1.2t^{1/2}$. We find the mean wavelength from our simulation results using the method described by Zimmerman & Homsy (1991) and Zimmerman (1991). We first obtain the power spectrum of the longitudinally averaged concentration profile and take the mean wavelength to be the inverse of the power-averaged wavenumber. The mean wavelengths $\lambda/2\pi$ obtained from our simulations using the above method do not asymptote to a linear function in $t^{1/2}$ but a least-square fit through the wavelengths closely follows the curve $\approx 1.0t^{1/2}$, which agrees with the experimental results to within 20%. Both the qualitative and quantitative features of our simulations compare favourably with those of Wooding's experiments.

5.2. *Fingering with both viscosity and density contrasts*

We study the effects of combined viscosity and density contrasts on the nonlinear evolution of the fingering instabilities. When both viscosity and density differences have a stabilizing effect on the flow, the flow is always stable. When they both act to destabilize, the flow is always unstable and the resulting fingers are qualitatively not very different from those driven solely by viscosity contrasts. The interesting cases are when the viscosity and density contrasts have opposite effects. In such cases, we can have regions that are locally stable followed downstream by regions that are locally unstable or vice versa. We confine our attention to the following two cases: (i) viscous stabilization of gravitational fingers and (ii) gravitational stabilization of viscous

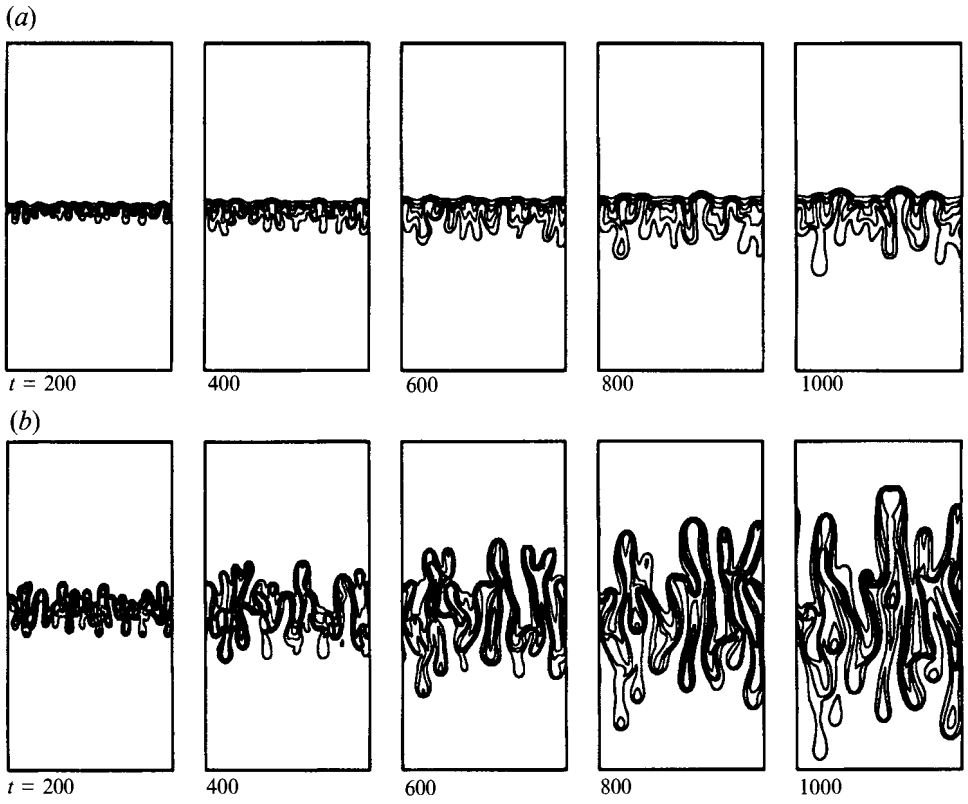

FIGURE 7. Viscous stabilization of gravitational fingers: (*a*) injection velocity $U = 1$, (*b*) injection velocity $U = 0$. The stabilizing viscosity contrast not only reduces the growth of fingers but also changes the direction of finger propagation. The concentration fields at various times are shown as contour plots with the contours spanning from $c = 0.9$ to 0.1 in six equal increments. The fluid pair has an exponential viscosity dependence with $\alpha = \mu_2/\mu_1 = 0.1$ and for both simulations $Pe = V_{ch}H/D = 1000$, $A = 2$.

fingers. The nonlinear finger propagation in these cases are presented in the rest of this section.

5.2.1. *Viscous stabilization of gravitational fingers*

The gravitational fingers shown in figure 6 can be stabilized through viscous forces by introducing a favourable viscosity contrast to the flow. A more viscous and heavier fluid is injected from the top to displace a less viscous and lighter fluid from the bottom. We consider the displacement with an unstable density contrast, $\Delta\rho > 0$ and a favourable viscosity ratio, $\alpha = 0.1$. For this choice of density and viscosity contrasts, the local critical velocity as a function of concentration and its spatial variation under one-dimensional dispersion are shown in figure 5. The flow develops an upstream stable zone and a downstream unstable zone when the injection velocity is between the upper and lower bounds of the local critical velocity $u_c(c)$, as indicated in figure 5. We simulate the flow with an injection velocity $U = 1$, which is between the lower and upper bounds of the local critical velocity. The results of the simulation are shown in figure 7(*a*) as concentration contours at various times. The concentration contours span from $c = 0.9$ to 0.1 in equal increments. For comparison, the propagation of fingers for the same viscosity and density profiles but with zero injection velocity is shown in figure 7(*b*).

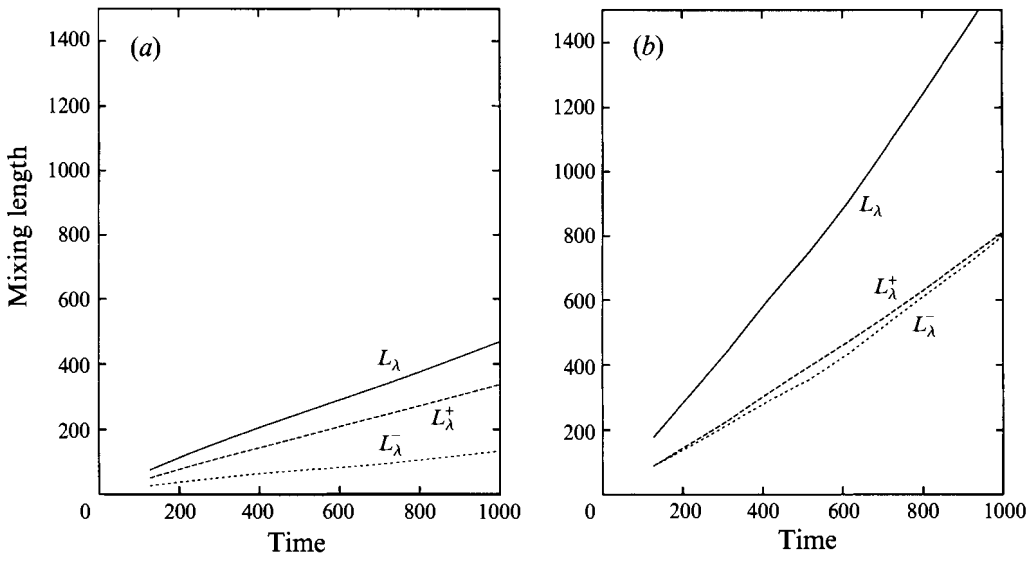

FIGURE 8. Growth of mixing lengths with time for the flow with injection velocity (*a*) $U = 1$ and (*b*) $U = 0$. The viscosity profile is exponential with $\alpha = \mu_2/\mu_1 = 10$.

When the injection velocity is zero, the flow is locally unstable everywhere and the fingers propagate as rapidly in either direction (figure 7*b*). Along an upward moving finger, low-viscosity fluid displaces high-viscosity fluid which results in steep concentration gradients and the fingers undergo tipsplitting secondary instabilities. When the fluid is injected downward with a velocity $U = 1$, the stabilizing viscous forces not only reduce the finger growth but also change the direction of finger propagation. The upstream stable zone acts as a barrier to finger propagation in the upward direction and the viscosity-stabilized gravitational fingers propagate predominantly in the downward direction as seen in figure 7(*a*). In the first three frames of figure 7(*a*), the $c = 0.9$ concentration contours (lowest contour in each frame) are highly contorted whereas the $c = 0.1$ concentration contours (highest contours in each frame) are hardly perturbed. At larger times, the fingers penetrate the stable zone but their growth is still restricted.

The streamwise growth of the fingers can be quantitatively characterized through mixing lengths. We use the integral definitions of Manickam & Homsy (1994) to define a forward (L_λ^+), a reverse (L_λ^-) and a total (L_λ) mixing length:

$$L_\lambda^+ = 3\int_{x_0}^{L} x\bar{c}(x)\,\mathrm{d}x \Big/ \int_{x_0}^{L} \bar{c}(x)\,\mathrm{d}x, \tag{12a}$$

$$L_\lambda^- = 3\int_{0}^{x_0} x[1-\bar{c}(x)]\,\mathrm{d}x \Big/ \int_{0}^{x_0} [1-\bar{c}(x)]\,\mathrm{d}x, \tag{12b}$$

$$L_\lambda = L_\lambda^+ + L_\lambda^-, \tag{12c}$$

where x_0 is the initial location of the interface and all measurements are in a reference frame moving with the injection velocity. The forward mixing length is a measure of the extent to which the displacing fluid has penetrated the displaced fluid while the reverse mixing length is a measure of the extent to which the displaced fluid has penetrated the displacing fluid. For the two sets of simulations shown in figure 7, the mixing lengths are plotted against time in figure 8. When the injection velocity is zero,

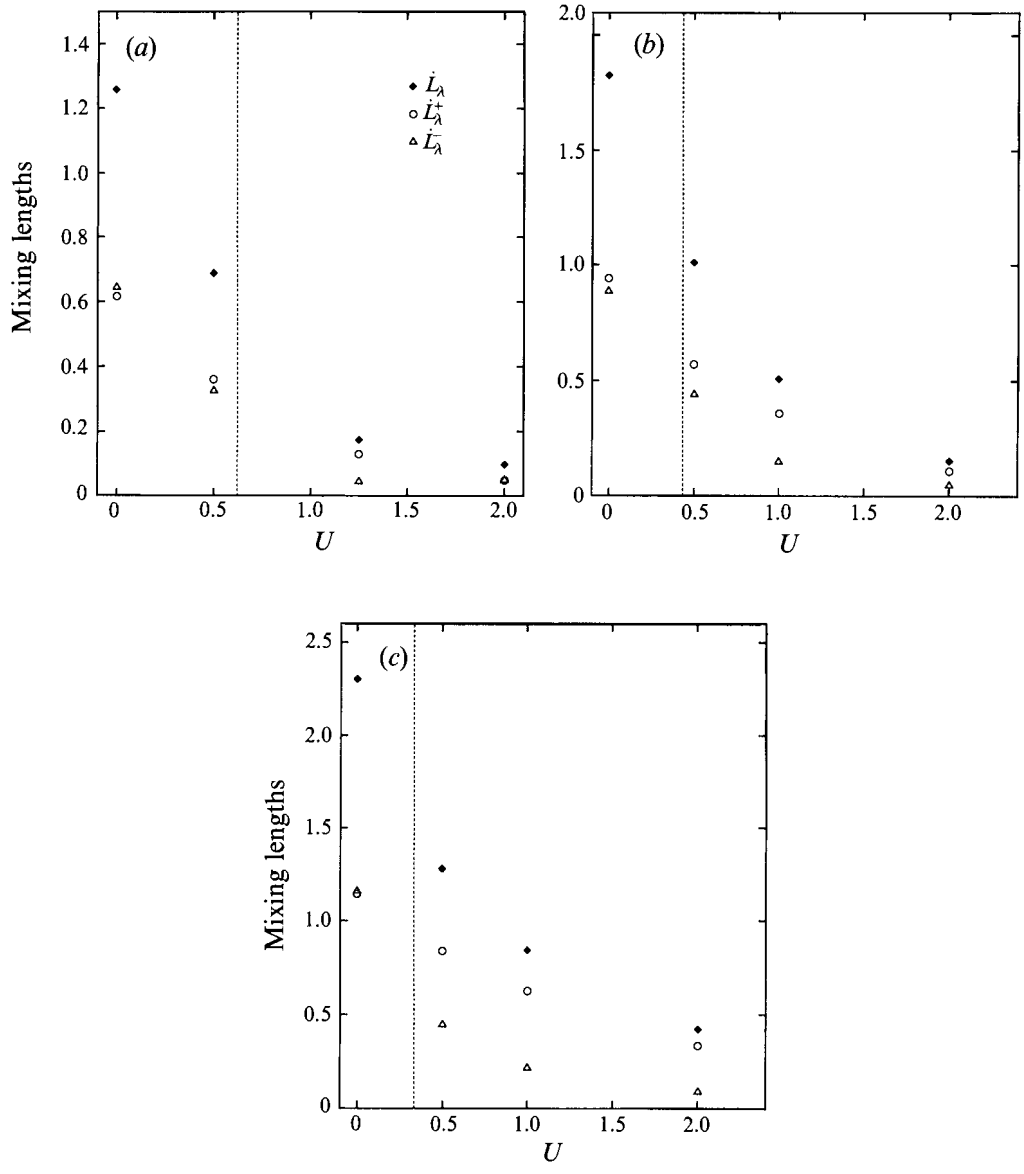

FIGURE 9. The dependence of mixing lengths on injection velocity for the gravitationally unstable but viscously stable flows. The density profiles are linear and the viscosity profiles are exponential with endpoint viscosity ratios (*a*) $\alpha = 0.2$, (*b*) $\alpha = 0.1$, (*c*) $\alpha = 0.05$. The lower limit of the local critical velocity is indicated by dashed lines in each plot. To the right of the dashed lines, the flow develops stable regions followed downstream by unstable regions.

the forward mixing length L_λ^+ is approximately equal to the reverse mixing length L_λ^- (figure 8*b*). When $U = 1$, the stabilizing viscous forces reduce the growth of mixing lengths in both the directions and the forward mixing length is always greater than the reverse mixing length.

In all our simulations, the time derivatives of the mixing lengths asymptote to nearly a constant. This allows us to define asymptotic mixing rates in the forward direction $\dot{L}_\lambda^+$, and in the reverse direction $\dot{L}_\lambda^-$ as the asymptotic values of the time derivatives of L_λ^+ and L_λ^- respectively. We define a total asymptotic mixing rate $\dot{L}_\lambda \equiv$

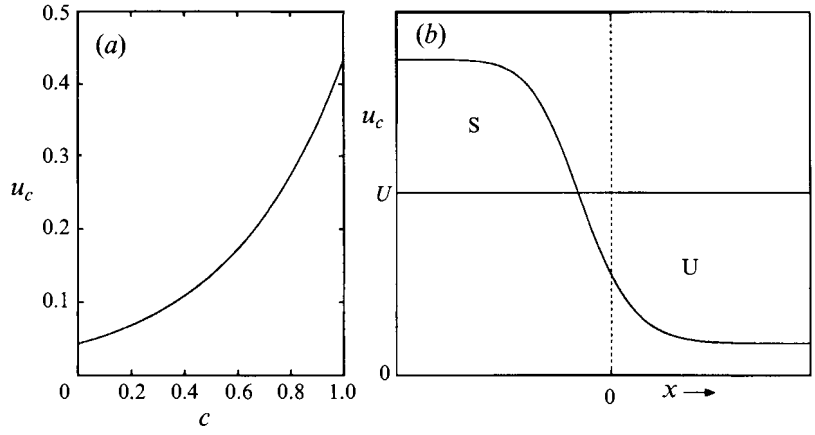

FIGURE 10. (*a*) The variation of local critical velocity u_c with concentration c for an unstable exponential viscosity profile with $\alpha = 10$ and a stable density stratification. (*b*) The corresponding spatial variation of the local critical velocity $u_c(x)$ under one-dimensional dispersion. The region marked S where $U > u_c$ is potentially stable and the region marked U where $U < u_c$ is potentially unstable.

$\dot{L}_\lambda^+ + \dot{L}_\lambda^-$, which (scaled with V_{ch}) when extracted from figure 8(*b*) for the $U = 0$ case is 1.83, and the ratio of forward to reverse mixing rates, $\dot{L}_\lambda^+/\dot{L}_\lambda^- \approx 1$. When stabilizing viscous forces are introduced by injecting at $U = 1$, the total asymptotic mixing rate is reduced by a factor of 4 and the ratio of forward to reverse mixing rates, $\dot{L}_\lambda^+/\dot{L}_\lambda^- \approx 2.5$. The up–down symmetry of the density-driven fingers is destroyed by the upstream stable barrier and the fingers propagate preferentially in the downward direction.

To further understand the effects of stabilizing viscous forces on the density-driven fingers, we parametrically study the dependence of the mixing rates with injection velocity. We choose the three favourable viscosity ratios, $\alpha = 0.2$, 0.1, 0.05, and simulate the flow at various injection velocities. The asymptotic mixing rates are extracted from each of these simulations and are plotted against injection velocity in figure 9(*a–c*) for the three viscosity ratios chosen. In each of the plots, the dashed line indicates the lower bound of the local critical velocity u_{cl} at injection velocities beyond which the flow develops locally stable regions.

For all three viscosity ratios considered, the finger patterns exhibits up–down symmetry when the injection velocity U is close to zero, with $\dot{L}_\lambda^+ \approx \dot{L}_\lambda^- \approx \dot{L}_\lambda/2$. When $U > u_{cl}$, the symmetry is destroyed and fingers propagate at a higher rate in the downstream direction than in the upstream direction, as evidenced by unequal values of $\dot{L}_\lambda^+$ and $\dot{L}_\lambda^+$. The locally stable region on the upstream direction is effective in altering the direction of finger propagation, especially at high viscosity contrasts ($\alpha = 0.05$ in figure 9). As the injection velocity is increased, the finger propagation is further skewed to the downstream direction. When the injection velocity approaches the upper bound of the local critical velocity, u_{cu}, the flow is stabilized and the growth of the mixing zones is controlled by dispersive rather than convective forces which again results in equal growth rate in either direction. Thus the ratio of forward to reverse mixing rates, $\dot{L}_\lambda^+/\dot{L}_\lambda^-$, a measure of the asymmetry in the finger propagation, is highest at some intermediate values of the injection velocity U, between the lower and upper bounds of the critical velocity. The flow is completely stabilized when the injection velocity exceeds the upper bound of the critical velocity.

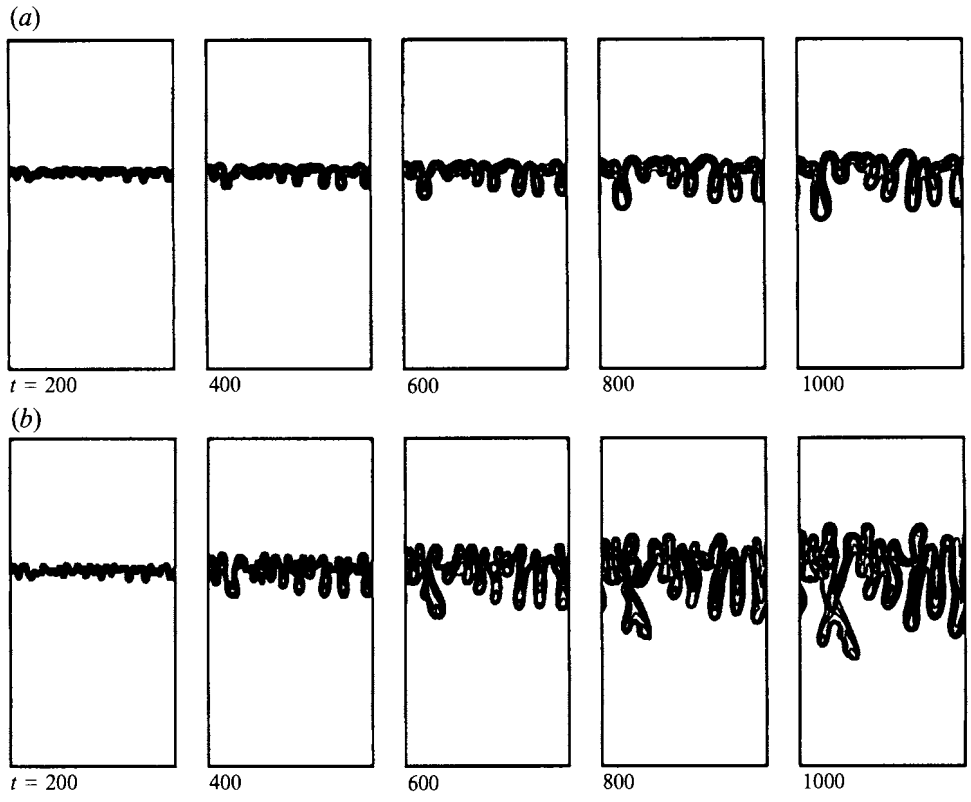

FIGURE 11. Viscous fingering in the presence and absence of stabilizing density effects: (*a*) stable density contrast $\Delta\rho g/\mu_1 U = -4$, (*b*) neutrally buoyant fluids $\Delta\rho = 0$. The viscosity profile is exponential with $\alpha = \mu_2/\mu_1 = 10$. The concentration fields at various times are shown as contour plots with the contours spanning from $c = 0.9$ to 0.1 in six equal increments. The velocities, lengths and time are scaled with the injection velocity U, D/U and D/U^2 respectively. For both the simulations, $Pe = UH/D = 1500$ and $A = 2$.

5.2.2. *Gravitational stabilization of viscous fingers*

We next consider the case where a less-viscous and lighter fluid is injected from the top to displace a more-viscous and heavier fluid from the bottom. When the injection velocity exceeds the lower bound of the critical velocity, the flow will become unstable. The viscous fingers that develop are stabilized by the density stratification in the flow. We choose the exponential viscosity profile (3) with an unfavourable viscosity ratio $\alpha = \mu_2/\mu_1 = 10$ and a stable density contrast $\Delta\rho < 0$. For this combination of viscosity and density profiles, the variation of the local critical velocity with concentration and the streamwise spatial variation under one-dimensional conditions are shown in figure 10.

The flow is potentially unstable in regions where $U > u_c$ and is potentially stable in regions where $U < u_c$. We simulate the flow with an injection velocity of $U = 0.25$ which, as shown in figure 10, is between the upper and lower bounds of the critical velocity and the flow develops a potentially stable region at the upstream end and a potentially unstable region at the downstream end of the transition zone. The results of the simulation are shown in figure 11(*a*) as snapshots of the concentration field at various times. In figure 11(*b*), the evolution of viscous fingers with neutrally buoyant fluids are shown for comparison. The gravity-stabilized flow shown in figure 11(*a*) is

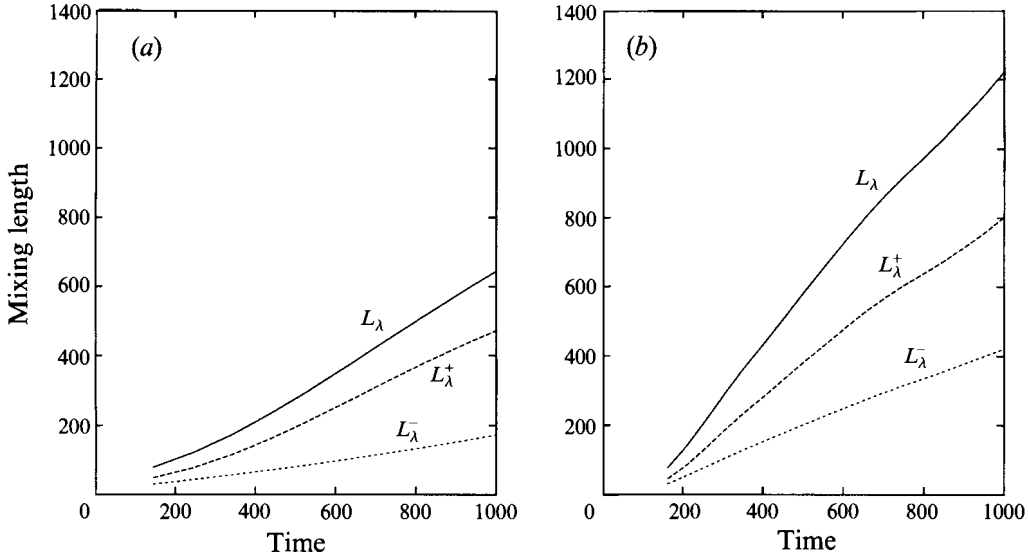

FIGURE 12. Growth of mixing lengths with time for the flow (*a*) with a stabilizing density stratification $\Delta\rho g/\mu_1 U = -4$, and (*b*) with neutrally buoyant fluids. The viscosity profile is exponential with $\alpha = \mu_2/\mu_1 = 10$.

scaled with the injection velocity U, instead of with the characteristic velocity V_{ch}, in order to aid a direct comparison with the neutrally buoyant case shown in figure 11(*a*). According to this scaling, the density contrast is $\Delta\rho g/\mu_1 U = -4$ and the length and time scales are D/U and D/U^2 respectively.

When the two fluids are neutrally buoyant (figure 11*b*), the instabilities develop into viscous fingers that readily undergo the nonlinear mechanisms (Tan & Homsy 1988) of spreading, shielding, coalescence and tipsplitting. When a stabilizing density stratification is added to the flow, the above mentioned fingering mechanisms are either suppressed or delayed in time. The upstream stable region curtails the reverse flow and the fingers propagate preferentially in the forward direction. The mixing lengths are plotted against time in figure 12 for the two simulations shown in figure 11. The density stratification has considerably reduced the growth of the mixing zones. The stabilizing buoyancy forces reduce the net force available to drive the fingers which results in a reduced rate of finger propagation. The viscous fingers with neutrally buoyant fluids (figure 12*b*) propagate primarily in the forward direction, with $L_\lambda^+ > L_\lambda^-$ at all times. When a stable density contrast is added to the flow (figure 12*a*), the presence of the upstream locally stable region further restricts the growth of the reverse mixing length.

We next parametrically study the effects of density contrasts on the viscous fingering instabilities. We choose the three unfavourable viscosity ratios $\alpha = 5$, 10 and 20 and simulate the displacement process with fluids of varying density contrasts. The asymptotic mixing rates obtained from each of the simulations are plotted against density contrasts in figure 13(*a–c*) for the three viscosity ratios. To the left of the dashed lines in each of the plots, the flow develops locally stable regions at the upstream end of the transition zone.

At low viscosity ratio $\alpha = 5$ (figure 13*a*), the stable and unstable zones are relatively weak and the flow is stabilized with moderate density contrasts ($\Delta\rho g/\mu U < -4$). The locally stable regions are not as effective in altering the direction of finger propagation as they are at high viscosity ratios. At higher viscosity ratios, the locally stable regions

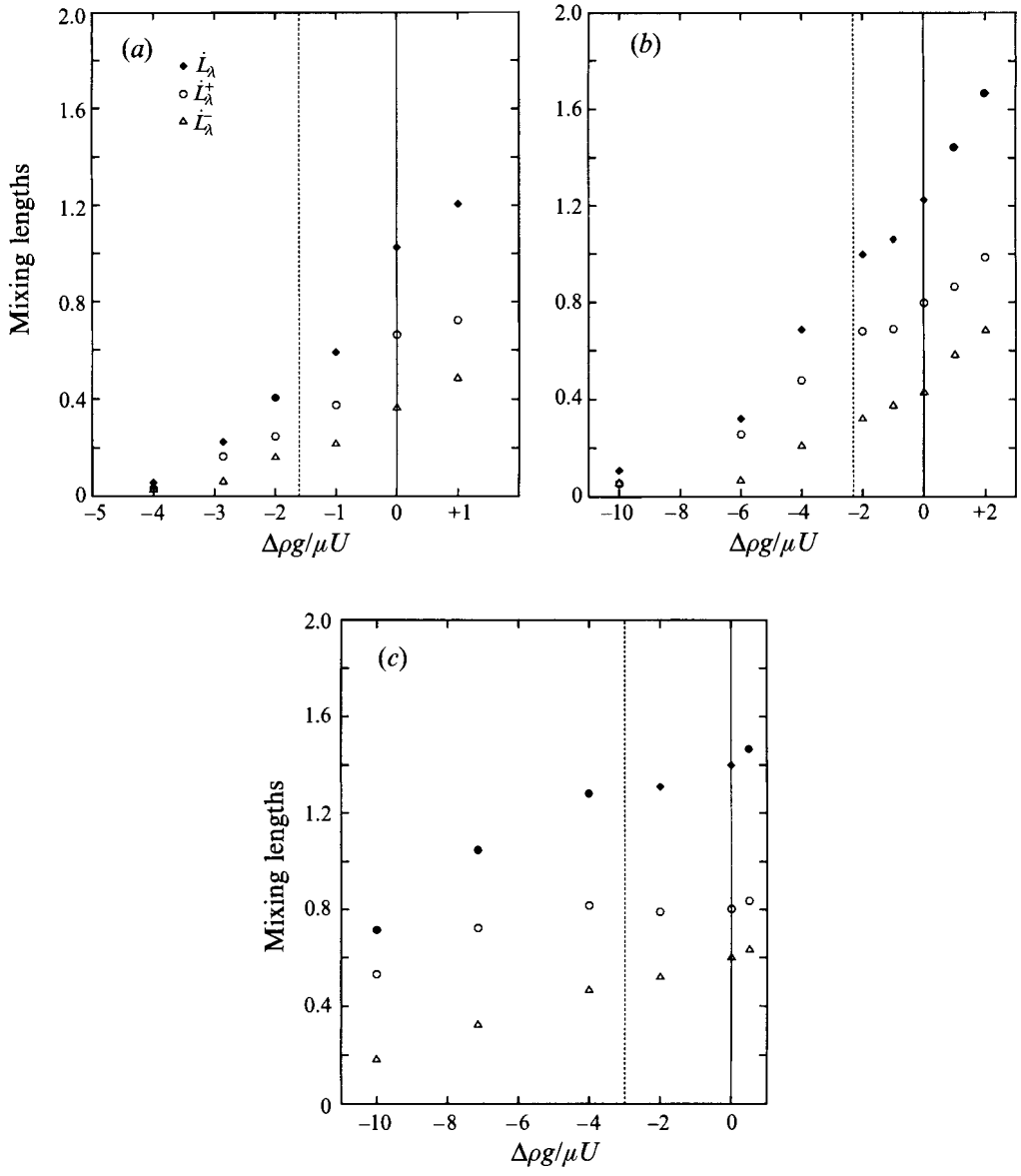

FIGURE 13. The dependence of mixing lengths on density difference for the viscously unstable but gravitationally stable flows. The density profiles are linear and the viscosity profiles are exponential with endpoint viscosity ratios (*a*) $\alpha = 5$, (*b*) $\alpha = 10$, (*c*) $\alpha = 20$. To the left of the dashed lines, the flow develops stable zones followed downstream by unstable zones.

restrict the reverse flow and increase the asymmetry in the direction of finger propagation. This is seen as an increase in the ratio of forward to reverse mixing rates, $\dot{L}_\lambda^+/\dot{L}_\lambda^-$, to the left of the dashed lines in figures 13(*b*) and 13(*c*). When $\alpha = 20$ (figure 13*c*), low density contrasts do not have any effect on the flow and it takes a much larger density contrast to completely stabilize the flow.

5.3. *Reverse fingering*

In our study thus far, the flow develops a locally stable zone at the *upstream* end of the transition zone. If the stable region is located at the *downstream* end, then the fingers

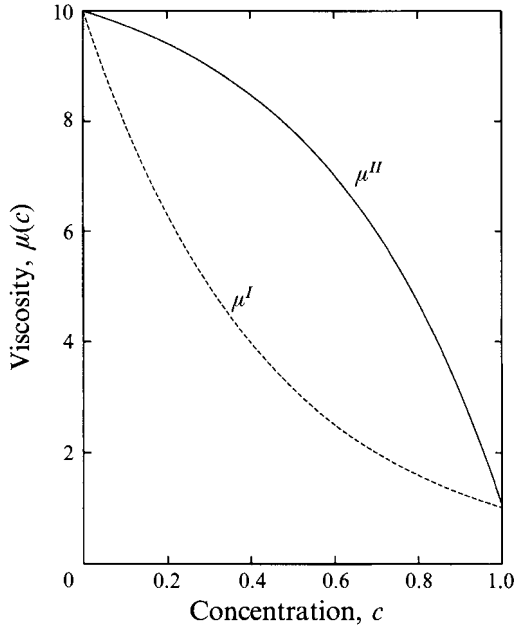

FIGURE 14. The two viscosity profiles $\mu^I = \exp(R(1-c))$ and $\mu^{II} = 1+\alpha-\exp(Rc)$ are compared for a viscosity ratio $\alpha = 10$.

would propagate preferentially in the reverse direction as they encounter a stable barrier in the forward direction, leading to the potential for 'reverse' fingering. Manickam & Homsy (1994) observed reverse fingering, where the displaced fluid penetrates the displacing fluid more readily than vice versa, in flows with spatially non-monotonic viscosity variations. Rogerson & Meiberg (1993) observed the same phenomena, which they referred to as 'backward' fingering, in vertical displacements with nonlinear density profiles. We can achieve a locally stable zone at the downstream end in vertical displacements by suitably choosing the viscosity profile. We use the linear density profile (2) as before, to be consistent with the incompressibility equation (1*a*), but choose the viscosity profile

$$\mu^{II} = 1+\alpha-\mathrm{e}^{Rc}, \tag{13}$$

where α is the endpoint viscosity ratio and is related to the constant R through $R = \ln\alpha$. The viscosity concentration relationships μ^{II} given in (13) and μ^I given in (3) are compared in figure 14 for a viscosity ratio $\alpha = 10$. The derivatives of the two profiles with respect to concentration are related through $\mu^{I\prime}(c) = \mu^{II\prime}(1-c)$ and the local critical velocities obtained with two profiles for the same density stratification are similarly related through $u_c(c;\mu^I) = u_c(1-c;\mu^{II})$. The upstream stable zones and the downstream unstable zones shown in figure 5 for flows with μ^I, switch places when μ^I is replaced with μ^{II}, as illustrated in figure 15(*a*).

The locally stable zone has the potential to act as a barrier to finger propagation in the downstream direction and the situation is conducive to reverse fingering. The strength and position of the stable region changes as the total local velocity changes in the flow, which leads to interesting flow dynamics. We demonstrate the phenomenon of reverse fingering in vertical displacements through two illustrative cases: (i) where the density-driven fingers are stabilized by viscous forces and (ii) where the viscous fingers are stabilized by density stratifications.

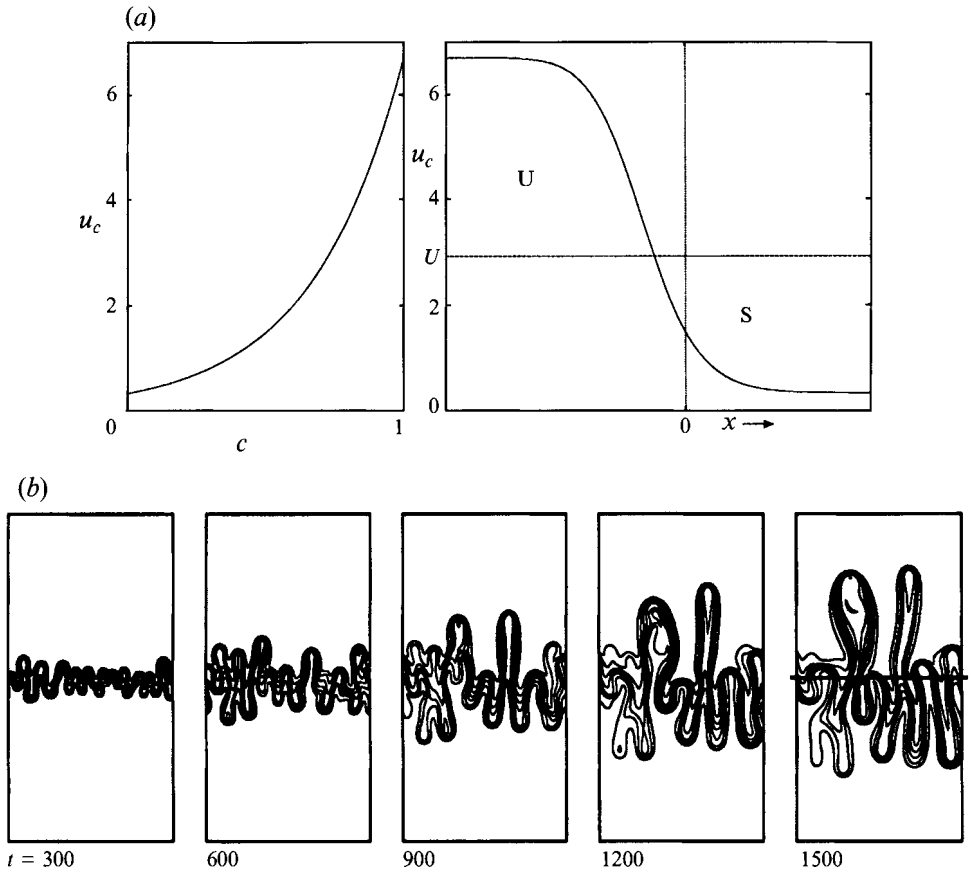

FIGURE 15. Reverse fingering in density-driven displacements ($\Delta\rho > 0$). The viscosity–concentration relationship is given in equation (13) with $\alpha = 0.1$. (*a*) Variation of *local* critical velocity with concentration and streamwise distance for the flow. (*b*) The concentration field at various times shows the finger propagation. The contours shown span from $c = 0.9$ to 0.1 in equal increments. The horizontal line in the last frame shows the initial location of the interface. The simulations are with $Pe = V_{ch} H/D = 1000$, $A = 2$.

We first simulate the case where a denser and less-viscous fluid is above a lighter and more-viscous fluid. We choose the linear density profile (2) with $\Delta\rho > 0$ and the exponential viscosity profile (13) with a favourable viscosity ratio $\alpha = 0.1$ and a zero injection velocity. The variations of local critical velocity with concentration and streamwise distance under one-dimensional conditions is shown in figure 15(*a*). The flow is locally stable in regions where the local total velocity exceeds the local critical velocity and is locally unstable in regions where the local total velocity is below the local critical velocity. The results of the simulation with zero injection velocity is presented in figure 15(*b*) as concentration contours at various times.

When the injection velocity is zero, the flow is locally unstable everywhere and the resulting finger patterns exhibit the characteristic up–down symmetry of density-driven flows, as seen at $t = 300$ and 600 in figure 15(*b*). As the flow evolves, the local total velocity increases and in some regions the local velocity exceeds the local critical velocity. Thus some fingers moving downward ($u > 0$) encounter a stable barrier (as indicated in figure 15*a*) at the tip whereas the fingers moving upward ($u < 0$) propagate with relative ease. The net result is that the upward moving fingers move faster than

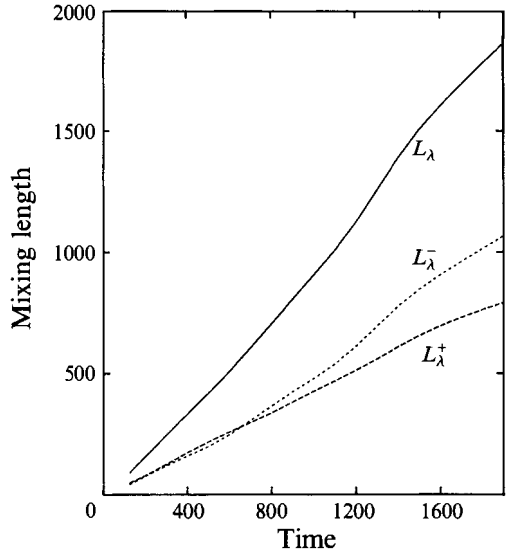

FIGURE 16. Growth of mixing lengths for the density-driven displacement with a stable viscosity contrast. The density profile is linear and the viscosity profile is given by equation (13) with $\alpha = 0.1$. At short times, the forward and the reverse mixing lengths grow at more or less the same rate but at later times the reverse mixing length grows at a higher rate than the forward mixing length.

their downward moving counterparts, leading to 'reverse' fingering. The initial symmetry in the direction of finger propagation and the subsequent reverse fingering are apparent in the mixing length versus time plot shown in figure 16. The forward (L_λ^+) and the reverse (L_λ^-) mixing lengths grow at the same rate until about $t = 800$, after which the reverse mixing length grows at a faster rate than the forward mixing length.

Similar to the density-driven flows, we can obtain reverse fingering in viscosity-driven instabilities. An illustrative case is shown in figure 17 where a less-viscous and lighter fluid is injected from the top to displace a more-viscous and heavier fluid. The viscosity varies with concentration according to (13) with a viscosity ratio $\alpha = 10$. The variation of local critical velocity with concentration and streamwise distance under one-dimensional dispersion is shown in figure 17(*a*). We simulate the flow with an injection velocity $U = 0.25$ and, as indicated in figure 17(*a*), the flow develops a locally stable region on the downstream side. The fingering instabilities are initiated in the unstable region and, owing to the stable barrier in the forward direction, they propagate preferentially in the reverse direction. However, as the local velocity increases, the downstream stable barrier becomes weaker and if the local velocity is high enough, a finger can 'penetrate' the stable barrier. One such instance is seen at $t = 1600$ in the simulations shown in figure 17(*b*). The local total velocity at which one of the fingers propagates approaches the upper limit of the local critical velocity, u_{cu}, and the finger penetrates the stable zone and propagates faster than the rest of the fingers. The mixing length versus time plot for the flow is shown in figure 18. Reverse fingering is evident from the plot as $L_\lambda^- > L_\lambda^+$ at all times. The forward mixing length, L_λ^+, grows at a slow rate until $t \approx 1200$, after which a finger breaks free and is reflected as a higher growth rate in L_λ^+.

The simulations shown in figures 15 and 17 demonstrate that reverse fingering can occur in vertical displacements with monotonic viscosity and density profiles, similar to what Manickam & Homsy (1994) obtained in horizontal displacements with non-

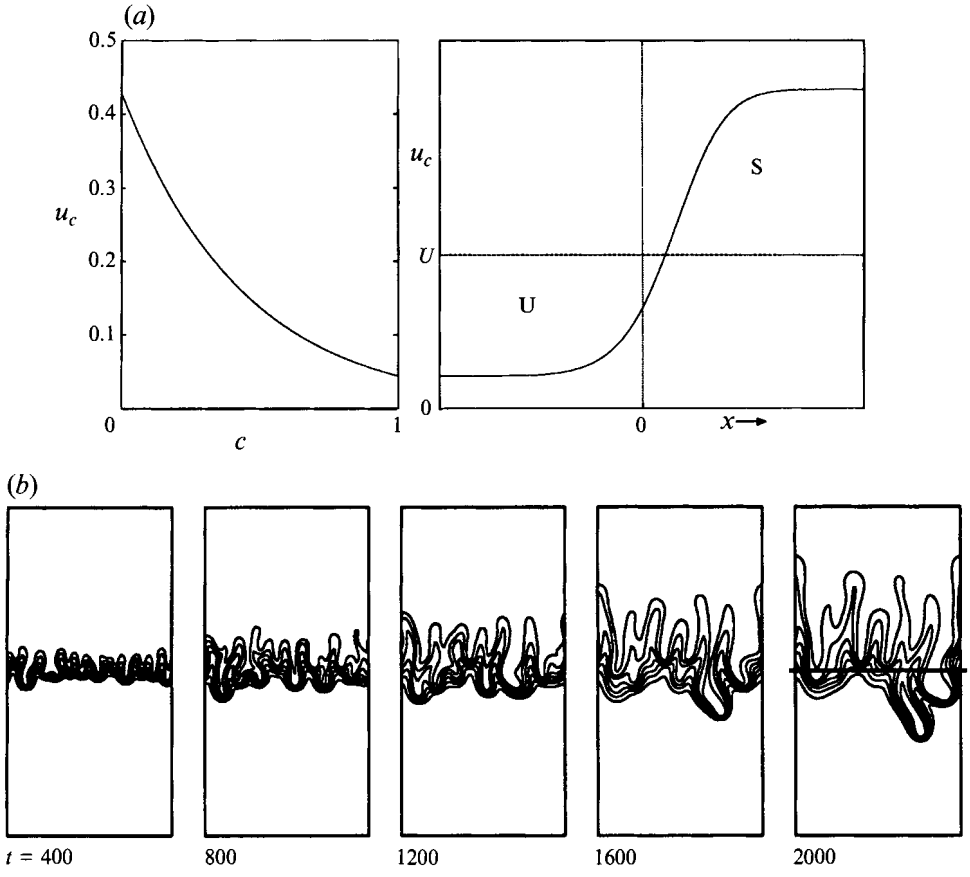

FIGURE 17. Reverse fingering in viscously unstable displacements with a stable density stratification. ($\alpha = 10$ and $\Delta\rho < 0$.) (*a*) Variation of *local* critical velocity with concentration and streamwise distance. (*b*) The finger patterns show reverse fingering and the penetration of a finger through the stable barrier. The concentration contours shown span from $c = 0.9$ to 0.1 in equal increments. The horizontal line in the last frame shows the initial location of the interface. The simulations are with $Pe = V_{ch}H/D = 1000$, $A = 2$.

monotonic viscosity profiles. In vertical flows, the strength and position of the stable barrier changes as the flow evolves which leads to more complex finger propagation than in horizontal flows.

6. Concluding remarks

We have analysed vertical miscible displacement flows with monotonic viscosity and density profiles using linear stability analysis and numerical simulations. The presence of density stratification can introduce regions that are locally stable, strikingly similar to horizontal flows with non-monotonic viscosity profiles. We have defined a *local* critical velocity and by comparing the local velocity field with the local critical velocity, the regions that are potentially stable and those that are potentially unstable can be identified. This simple method of identifying regions where the flow is potentially stable and unstable is very useful in interpreting the flow dynamics.

We have established that for a linear density profile, the displacements against the

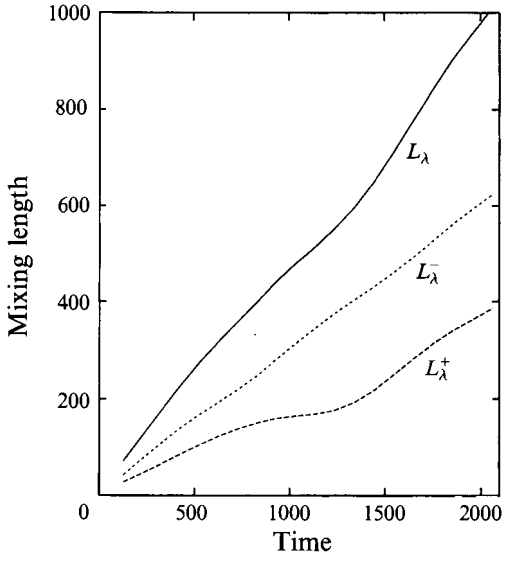

FIGURE 18. Mixing lengths plotted against time for the flow with a viscosity profile given by equation (13) with $\alpha = 10$ and a stable linear density profile. At short times, the growth in the forward direction is restricted by the stable barrier but once a finger penetrates the stable barrier, the forward mixing length grows at a higher rate.

direction of gravity are equivalent to the displacements along the direction of gravity and when both the viscosity and density profiles are linear, the vertical displacements are no different from the horizontal displacements. Our linear analysis shows that flows under gravity that are predicted to be stable by the step profile analysis can become unstable as the base state diffuses out. This is an example where diffusion can act to destabilize the flow and the step profile results are potentially misleading. The critical velocity obtained using the step profile analysis changes as the two fluids disperse into each other.

We have simulated the vertical displacement flow in two dimensions using a Hartley-transform-based spectral method and compared our simulation results with the experiments of Wooding (1969). The growth rates of the fingered zones and the finger widths obtained from our simulations agree to within 20% of the corresponding experimental measurements. When the density profile is linear, the fingering instabilities driven solely by density contrasts have no preferred direction of propagation. The fingers propagate at the same rate and through the same mechanisms at either end of the fingered zone. When a viscosity contrast is added to the flow, locally stable regions can be introduced by suitably choosing the viscosity profile and injection velocity. We have parametrically studied the effects of the stable zones on finger propagation for the class of flows where the stable regions develop at the upstream end of the transition zone. The locally stable zones act as effective barriers to reverse flow and the fingers propagate preferentially in the forward direction. The effects are more pronounced at high viscosity ratios than at low visosity ratios. Through a proper choice of viscosity profile and injection velocity, not only the rate of finger propagation but also the direction of finger propagation can be altered.

We have demonstrated through illustrative examples, the phenomenon of reverse fingering, where the displaced fluid fingers through the displacing fluid more easily than vice versa, by introducing a potentially stable region at the downstream end of the

transition zone. The position and strength of the stable zone changes as the flow evolves, leading to interesting finger propagation where some fingers encounter stable barriers while others propagate with relative ease.

We thank the US Department of Energy, Office of Basic Energy Sciences (Grant No. DE-FG03-87ER13673) for financial support and the San Diego Supercomputer Center (SDSC) for the time on the CRAY Y-MP.

REFERENCES

BACRI, J. C., SALIN, D. & YORTSOS, Y. 1991 Analyse lineaire de la stabilité de l'écoulement de fluides miscibles en milieux poreux. *C. R. Acad. Sci. Paris* **314**, 139.

BEAR, J. 1972 *Dynamics of Fluids in Porous Media*. Dover.

BRACEWELL, R. N. 1984 The fast Hartley transform. *Proc. IEEE* **72**, 1010.

BRACEWELL, R. N. 1986 *The Hartley Transform*. Oxford University Press.

BUNEMAN, O. 1987 Multidimensional Hartley transforms. *Proc. IEEE* **75**, 267.

CHRISTIE, M. A., JONES, A. D. W. & MUGGERIDGE, A. H. 1989 Comparison between laboratory experiments and detailed simulations of unstable miscible displacement influenced by gravity. Presented at *2nd Intl Conf. on North Sea Oil and Gas Reservoirs, Trondheim, Norway*.

CHIKHLIWALA, E. D., HUANG, A. B. & YORTSOS, Y. C. 1988 Numerical study of the linear stability of immiscible displacement processes in porous media. *Transport Porous Media* **3**, 257.

CHRISTIE, M. A., MUGGERIDGE, A. H. & BARLEY, J. J. 1991 3D simulation of viscous fingering and WAG schemes. *SPE* 21238. Presented at the *11th Symp. on Reservoir Simulation, Anaheim, California*, Feb 17–20.

COSKUNER, G. & BENTSEN, R. G. 1990 An extended theory to predict the onset of viscous instabilities for miscible displacements in porous media. *Transport Porous Media* **5**, 473.

DUMORE, J. M. 1964 Stability consideration in downward miscible displacements. *Soc. Petrol. Engrs J.* December, 356.

FAYERS, F. J. & NEWLEY, T. J. 1988 Detailed validation of an empirical model for viscous fingering with gravity effects. *Soc. Petrol. Engrs Reservoir Engng*, May, 542.

HICKERNELL, F. J. & YORTSOS, Y. C. 1986 Linear stability of miscible displacement processes in porous media in the absence of dispersion. *Stud. Appl. Maths* **74**, 93.

HILL, S. 1952 Channeling in packed columns. *Chem. Engng Sci.* **1**, 247.

HOMSY, G. M. 1987 Viscous fingering in porous media. *Ann. Rev. Fluid Mech.* **19**, 271.

JOSEPH, D. D. 1990 Fluid dynamics of two miscible liquids with diffusion and gradient stresses. *Eur. J. Mech.* B/*Fluids* **9**, 565.

MANICKAM, O. 1994 Viscous fingering in miscible displacements in porous media with non-monotonic viscosity profiles. PhD thesis, Stanford University.

MANICKAM, O. & HOMSY, G. M. 1993 Stability of miscible displacements in porous media with non-monotonic viscosity profiles. *Phys. Fluids* A **5**, 1356.

MANICKAM, O. & HOMSY, G. M. 1994 Simulation of viscous fingering in miscible displacements with non-monotonic viscosity profiles. *Phys. Fluids* **6**, 95.

ROGERSON, A. & MEIBURG, E. 1993 Numerical simulation of miscible displacement processes in porous media flows under gravity. *Phys. Fluids* A **5**, 2644.

TAN, C. T. 1987 Stability of miscible displacements in porous media. PhD thesis, Stanford University, Stanford.

TAN, C. T. & HOMSY, G. M. 1986 Stability of miscible displacements in porous media: Rectilinear flow. *Phys. Fluids* **29**, 3549.

TAN, C. T. & HOMSY, G. M. 1988 Simulation of non-linear viscous fingering in miscible displacement. *Phys. Fluids* **31**, 1330.

TCHELEPI, H. A. & ORR, F. M. 1993 The interaction of viscous fingering, permeability heterogeneity and gravity segregation in 3D. *SPE 25235*. Presented at the *12th SPE Symp. on Reservoir Simulation, New Orleans, Louisiana, February 28*.

TCHELEPI, H. A., ORR, F. M., RAKOTOMALALA, N., SALIN, D. & WOUMEÉNI, R. 1993 Dispersion, permeability heterogeneity and viscous fingering: Acoustic experimental observations and particle-tracking simulations. *Phys. Fluids* A **5**, 1558.

TIFFIN, D. L. & KREMESEC, V. J. 1986 A mechanistic study of gravity-assisted CO_2 flooding. *SPE/DOE* 14895. Presented at *SPE/DOE 5th Symp. on Enhanced Oil Recovery, Tulsa, Oklahoma, April 20.*

TRYGGVASON, G. & AREF, H. 1983 Numerical experiments on Hele-Shaw flow with a sharp interface. *J. Fluid Mech.* **136**, 1.

WOODING, R. A. 1969 Growth of fingers at an unstable diffusing interface in a porous medium or Hele-Shaw cell. *J. Fluid Mech.* **39**, 477.

YORTSOS, Y. C. & ZEYBEK, M. 1988 Dispersion driven instability in miscible displacement in porous media. *Phys. Fluids* **31**, 12.

ZIMMERMAN, W. B. 1991 Effects of the 3-D tensor character of dispersion on the viscous fingering instability in miscible displacement. PhD thesis, Stanford University, Stanford.

ZIMMERMAN, W. B. & HOMSY, G. M. 1991 Nonlinear viscous fingering in miscible displacement with anisotropic dispersion. *Phys. Fluids* A **3**, 1859.

ZIMMERMAN, W. B. & HOMSY, G. M. 1992 Three-dimensional viscous fingering: a numerical study. *Phys. Fluids* A **4**, 1901.